Single Magnetic Bead Detection in a Microfluidic Chip Using Planar Hall Effect Sensor

Hyuntai Kim, Venu Reddy, Kun Woo Kim, Ilgyo Jeong, Xing Hao Hu, and CheolGi Kim*

Department of Materials Science and Engineering, Chungnam National University, Daejeon 305-764, Korea

In this study, we fabricate an integrated microfluidic chip with a planar Hall effect (PHE) sensor for single magnetic bead detection. The PHE sensor was constructed with a junction size of 10 μm × 10 μm using a trilayer structure of Ta(3 nm)/NiFe(10 nm)/Cu(1.2 nm)/IrMn(10 nm)/Ta(3 nm). The sensitivity of the PHE sensor was 19.86 μV/Oe. A diameter of 8.18 μm magnetic beads was used, of which the saturation magnetization was ~2.1 emu/g. The magnetic susceptibility χ of these magnetic beads was calculated to be ~0.14. The diluted magnetic beads solution was introduced to the microfluidic channel attributing a single bead flow and simultaneously the PHE sensor voltage was measured to be 0.35 μV. The integrated microchip was able to detect a magnetic moment of 1.98×10^{-10} emu.

Keywords : planar Hall effect sensor, trilayer structure, single magnetic bead detection, microfluidics

1. Introduction

In magnetic sensing bioassay, the magnetic microbeads or nanoparticles are labeled with biomolecules (proteins, nucleic acids etc.) and are employed in detecting target biomolecules by binding the probe biomolecules immobilized on the magnetic sensor surface. In the literature, the magnetic sensing bioassay research has mainly focused on improving the limits of detection [1-3]. The improvement of the detection limit is attributed to the detection of very weak magnetic fields generated from the small number of conjugated magnetic biolabels (e.g single bead) on the magnetic sensor surfaces [4-6].

In this context, many types of magnetoresistive sensors have been developed for these bio-applications such as a giant magnetoresistive (GMR), a planar Hall effect (PHE) sensor, a semiconductor Hall sensor, and an anisotropic magnetoresistive ring (AMR) sensor [7]. Among them, the PHE sensors have gained more interest in the field of high sensitive magnetic biosensors because of their high-field sensitivity and very high signal-to-noise ratio properties [5]. In addition, the PHE sensors are also used in the applications of a microcompass for nanotesla detection, magnetic random access memory, and angular detec-

tion sensors [8-10].

In our early research work, we have demonstrated that the spin-valve planar hall sensor is capable of detecting the single bead by dropping the magnetic bead solution using a pipette on the sensor surface [5]. For biosensing applications, the magnetic bead labeled with biomolecules is introduced onto the sensor and then incubated prior to the washing steps. To achieve reproducible results under these conditions (incubating and washing steps), it is extremely important to integrate the microfluidic system on the PHE sensors. In addition, the microfluidic system provides systematic positioning of single beads on the PHE sensor. Microfluidic valves, pumps, and mixers can be added to the microfluidic system with the PHE sensor, which can provide an automated and complex analytical device [11].

In this work, we have performed an experiment to illustrate the possibility of single magnetic bead detection using an integrated microchip with microfluidic channel and PHE sensor. The simulation results of the stray field of the magnetic bead correlated well with the experimental data and provided information on the distance between the sensor and the magnetic bead. The detection limit of this system was calculated from the magnetic properties of the bead and the signal.

*Corresponding author: Tel: +82-42-821-6236
Fax: +82-42-822-6272, e-mail: cgkim@cnu.ac.kr

2. Experiment

2.1. Fabrication of a microfluidic chip integrated with a magnetic sensor

A trilayer PHE sensor with the junction size of 10 μm × 10 μm was patterned on a glass wafer using photoresist AZ 5214E (MicroChemicals, Germany) with conventional photolithography and the lift-off method [12]. First, the glass wafer was cleaned using methanol in an ultrasonic cleaner for 30 min., and washed with distilled water prior to drying with N_2 gas. An active sensing junction of 10 μm × 10 μm was stenciled on the photoresist (PR) at 1.6 μm thicknesses by first rinsing the glass wafer substrate in developer and rinsing again in deionized water.

Second, a typical trilayer structure of Ta(3 nm)/NiFe(10 nm)/Cu(1.2 nm)/IrMn(10 nm)/Ta(3 nm) was sputtered on the stencilled sensing junction of the 10 μm × 10 μm glass wafer using a DC magnetron sputtering system under a working pressure of 3 m Torr. During the deposition, a uniform magnetic field of 100 Oe was applied in the film plane to induce a magnetic anisotropy of ferromagnetic (FM) layers and to align the pinning direction of the anti-ferromagnetic (AFM) IrMn layer, which fixed the easy axis of the sensor to that direction and reduced the thermal noise. The photoresist was removed using a lift-off process, leaving the trilayer sensing junction of a 10 μm × 10 μm structure on the glass wafer substrate.

Then, using a similar photolithography, lift-off method process, and DC magnetron sputtering as those described above, Ta (10 nm)/Au (150 nm) electrodes were fabricated to connect the sensor junctions with the measuring electronic circuitry. Finally, the sensor junctions and electrodes were passivated with a layer of SiO_2 of 150 nm thickness using RF magnetron sputtering to protect the sensor junctions and electrodes from corrosion in the fluidic system.

The microfluidic channels were prepared using a soft lithography procedure [13]. Briefly, a master for the channel a master with a width of 50 μm and thickness of 15 μm was prepared on a silicon wafer with SU-8 50 PR by using a negative pattern film mask. Polydimethylsiloxane (PDMS) components in a 10:1 w/w ratio (Sylgard 184) of base to curing agent were poured on the master and cured thermally at 75 °C for 1 h. The solidified PDMS micro-fluidic stamp was lifted from the master and punched to create the inlet and outlet.

The resulting PDMS stamp was aligned and bonded on the magnetic sensor after being treated with a plasma cleaner (CUTE, FEMTO SCIENCE, Korea) for 90 sec at 0.5 Torr of oxygen and 100 Watts, and was then transferred to a preheated oven maintained at 75 °C for 1 h. The resulting microchip with microfluidic channel and a PHE sensor is shown in Fig. 1a. A microscopic image of a fabricated PHE sensor in a microfluidic channel is shown in Fig. 1b.

2.2. Characterization of magnetic beads

The magnetic beads of 8.18 μm diameter were procured from Bangs Laboratories, Inc. (IN, USA). The magnetic properties of the magnetic beads were measured at room temperature using the Lake-Shore 7407 series vibration sample magnetometer (VSM) with a sensitivity of 10^{-6} emu. The surface morphology and microstructure of the magnetic beads were observed by Field emission scanning electron microscope (FE-SEM, Nova-230) with an operating voltage of 10 kV.

2.3. Sensor characterization

Fig. 1c shows the uniaxial anisotropy field of the tri-layer structure and/or the unidirectional anisotrophy field H_{ex} is aligned parallel to the y-direction. The profiles of the PHE sensor signals were measured using electrodes along the x-axis at a sensing current of 1 mA under external magnetic fields ranging from −20 Oe to +20 Oe applied perpendicular to the direction of current. The uniform magnetic field was applied from the Helmholtz coil, which was controlled by the LabVIEW computer program. A Nanovoltmeter (Keithley, 2182A, USA) with sensitivity of 10 nV was used to measure the induced output voltages. All these PHE sensor characterizations
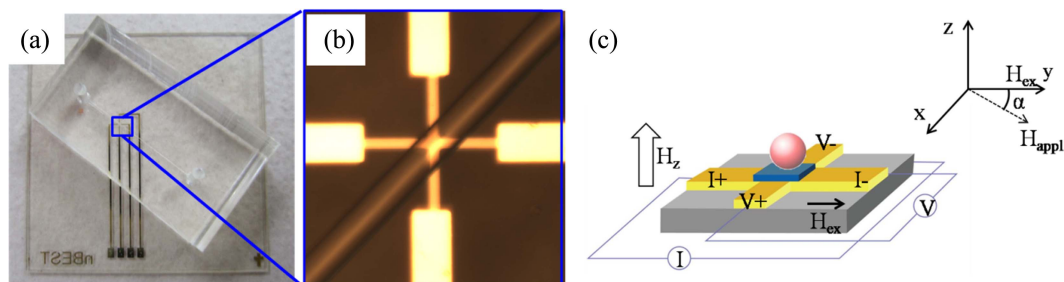

Fig. 1. (Color online) (a) Integrated microfluidic chip with a PHE sensor. (b) Microscopic image of a fabricated PHE sensor in a microfluidic channel. (c) Schematic view of PHE sensor voltage and current line orientations.
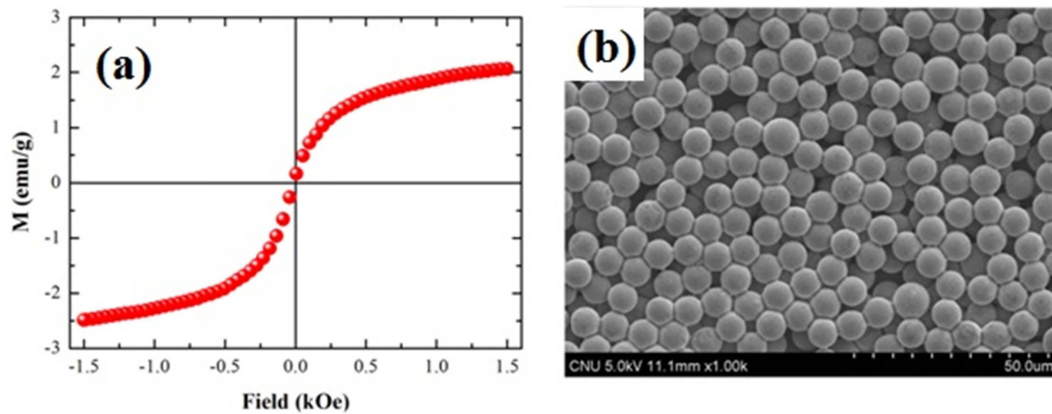
Fig. 2. (Color online) (a) VSM curve and (b) SEM image of magnetic beads with a diameter of 8.18 μm.

were carried out at room temperature. Fig. 1c also represents the PHE sensor voltage and current line connection orientations.

2.4. Measurement setup

In this work, we used the monitoring setup which was reported earlier [13]. Briefly, the microfluidic chip was placed at the centre between two Helmholtz coil systems for the generation of a uniform magnetic field. A 5 mA current was applied to the PHE sensor using a current source. A system was designed for injecting a diluted solution of magnetic beads with a diameter of 8.18 μm
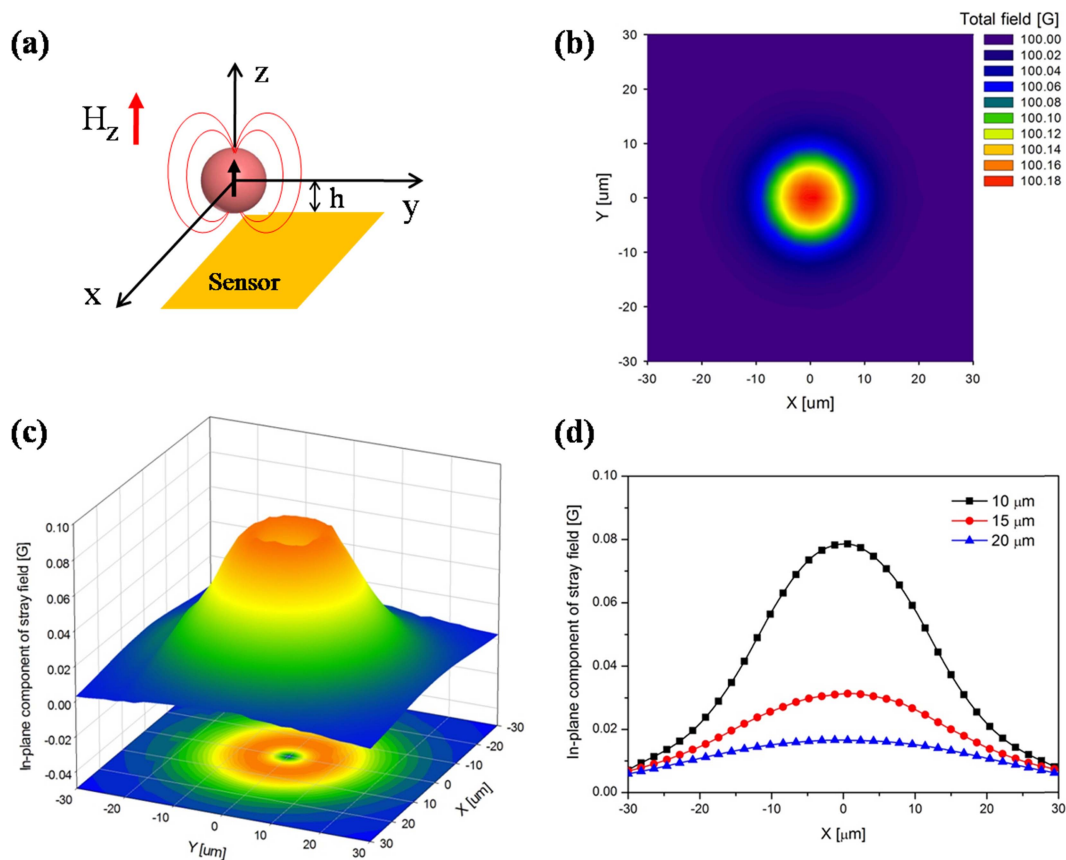

Fig. 3. (Color online) Simulation results of the stray field of a single magnetic bead with a diameter of 8.18 um under an applied field of 100 Oe. (a) Schematic view of the single bead and plane (sensor surface). (b) Contour of total field on the plane at a distance of 10 μm from the bead. (c) Graphical depiction of in-plane component of bead stray field on the plane at a height of 10 um from the bead. (d) Maximum in-plane component of stray field along the *x*-axis at different heights from the bead.

into the microfluidic channel using tubing attached to the inlet and outlet of the microfluidic chip. The flow of magnetic beads in the microfluidic channel over the sensor surface was observed using a microscope connected to a computer. The change in output voltage from the response of the passing single magnetic bead over the PHE sensor was measured using aNanovoltmeter.

3. Results and Discussion

3.1. Characterization of magnetic beads

Fig. 2a shows the magnetic hysteresis loop of magnetic beads with a diameter of 8.18 µm. The sample shows superparamgnetic properties, negligible coercivity, and negligible remanent magnetization. The saturation magnetization of these beads is approximately 2.1 emu/g. From this curve, the susceptibility χ of magnetic beads with 8.18 µm is calculated to be ~0.14, corresponding to the core volume and polymer volume of the bead as ~2% and ~98%, respectively. Fig. 2b shows the SEM image of the magnetic beads. The mean diameter of the magnetic beads is 8.18 µm. This result concurs with the company information provided.

3.2 Simulation of the magnetic field from a magnetic bead

A finite element method (FEM) simulation using Maxwell software (Ver. 12.2, Ansoft, USA) was used to analyze the stray field of a single magnetic bead. The magnetic field at a distance from a magnetic bead was calculated along with the magnetic properties (Fig. 3). The PHE sensor is sensitive to the in-plane field. A higher applied magnetic field causes a larger magnetic moment of the bead, which induces more stray field. However, the maximum applied magnetic field is limited by the saturation field of the sensor ~20 Oe. Thus, a 100 Oe perpendicular field was applied to induce the magnetic moment of the bead (Fig. 3a), but the in-plane component of the stray field was calculated for the estimation of the sensor signal as shown in Figs. 3(c-d). The saturation magnetization of the magnetic beads is about 28 emu/cc with the bead density of 1.08 g/cc.

The taper contour of the total field is obtained on the plane at a distance of 10 µm from the bead corresponding to the sensor surface, in which the maximum field is at the center (Fig. 3b). However, the contour of the in-plane component of the stray field of the single bead is not a taper, but a volcano configuration as shown in Fig. 3c. The maximal in-plane component of the stray field at one quarter distance from the bead center is shown in Fig. 3d, in which the field displays single peak. The intensity of
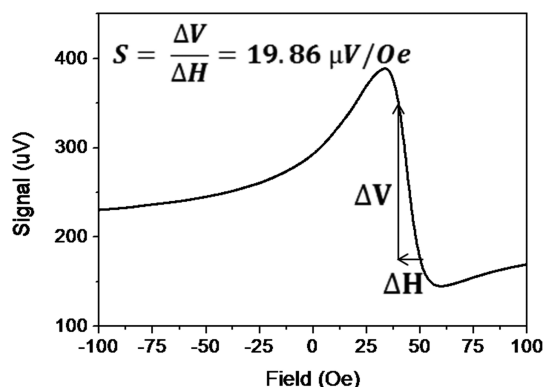

Fig. 4. Measured PHE sensor voltage profile.

the single peak is decreased by increasing the distance between the bead and sensor.

3.3. Detection of single magnetic bead

Fig. 4 shows the PHE sensor signal profile for an applied field angle, $\alpha \approx 20°$. Based on this curve, the sensitivity S of the signal was calculated to be 19.86 µV/Oe. The microscopic images and signal from the single magnetic bead were captured and measured simultaneously in the experimental set up, as shown in Fig. 5. The
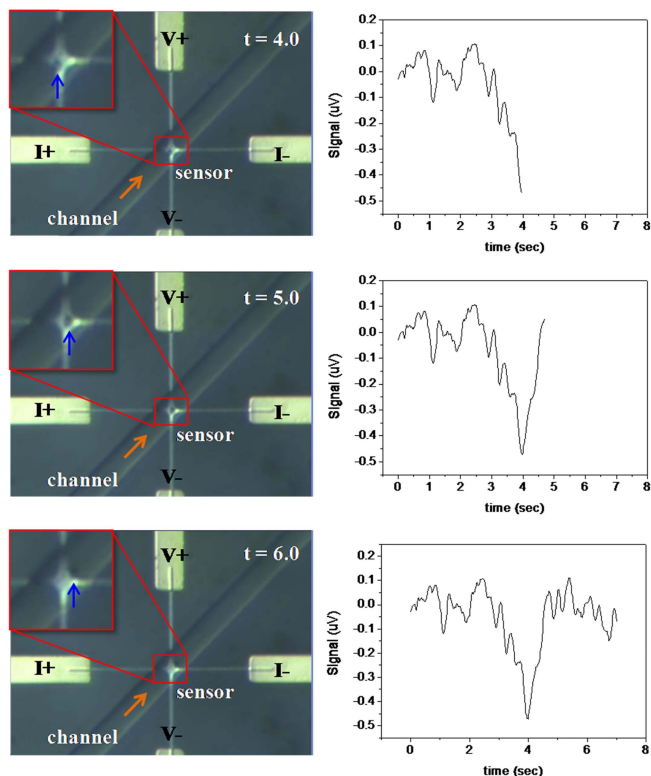

Fig. 5. (Color online) Images of single magnetic bead flowing over a PHE sensor captured at different times (left side) and their corresponding out-put voltage graphs (right side).

signal maximum value is approximately $\Delta V = 0.35$ μV by the subtraction of noise value around ± 0.2 μV (Fig. 5). As expected from the simulation data (Fig. 3d), the experimental signal also displayed a single peak. The stray field of the magnetic bead value of the experiment signal is measured to be 0.02 Oe from the relationship, $\Delta H = \Delta V/S$. In the simulation data, this value falls in the region between 15 and 20 μm (Fig. 3d). Thus, the height of the magnetic bead from the sensor needs to be greater than 15 μm. This finding suggests a relatively large distance between the magnetic bead and the sensor. In the simulation data, additional experiments with various heights of the bead from the sensor in the microfluidic channel also provide clear comparisons (Fig. 3d).

The induced magnetic moment from the single bead is approximately 2.98×10^{-10} emu at 100 Oe. The signal intensity is 0.35 μV (Fig. 5). The measurable minimum signal of this system is 0.2 μV (noise level), thus it is possible to detect an induced magnetic moment as low as 1.98×10^{-10} emu. However, further research is needed to detect these lower levels of magnetic fields. This could be possible by developing an advanced measurement setup for noise level reduction.

4. Conclusions

We have successfully detected a single magnetic bead in an integrated chip microfluidic chip with a trilayer based PHE sensor. The distance between the magnetic bead and the magnetic sensor was calculated by simulating using Maxwell 3D software. These calculations suggest that the distance between the magnetic bead and sensor is large (greater than 15 μm). The magnetic susceptibility of the single bead with a diameter of 8.18 μm is measured to be 0.14, and the detection limit of the sensor is 1.98×10^{-10} emu. This study demonstrates the possibility of monitoring the magnetic moment of individual magnetic beads in a microfluidic channel by using a PHE sensor.

References

[1] B. Srinivasan, Y. Li, Y. Jing, Y. Xu, X. Yao, C. Xing, and J. Wang, Angew. Chem. Int. Ed. **48**, 2764 (2009).
[2] G. Li, S. Sun, R. J. Wilson, R. L. White, N. Pourmand, and S. X. Wang, Sens. Actuators A **126**, 98 (2006).
[3] C. R. Tamanaha, S. P. Mulvaney, J. C. Rife, and L. J. Whitman, Biosens. Bioelectron. **24**, 1 (2008).
[4] X. J. A. Janssen, L. J. van Ijzendoorn, and M. W. J. Prins, Biosens. Bioelectron. **23**, 833 (2008).
[5] T. Q. Hung, S. Oh, J.-R. Jeong, and C. G. Kim, Sens. Actuators A **157**, 42 (2010).
[6] P. P. Freitas, R. Ferreria, S. Cardoso, and F. Cardoso, J. Phys.: Condens. Matter **19**, 165221 (2007).
[7] P. P. Freitas, H. A. Ferreira, D. L. Graham, L. A. Clarke, M. D. Amaral, V. Martins, L. Fonseca, and J. S. Cabral, in: M. Johnson (Ed.), Magnetoelectronics, Elsevier, Amsterdam, 2004.
[8] Francois Montaigne, A. Schuhl, F. Nguyen Van Dau, and A. Encinas, Sens. Actuators A **81**, 324 (2000).
[9] Y. Bason, L. Klein, J. B. Yau, X. Hong, J. Hoffman, and C. H. Ahn, J. Appl. Phys. **99**, R701 (2006).
[10] M. Volmer, J. Neamtu, Physica B **403**, 350 (2008).
[11] I. Jeong, Y.-J. Eu, K. W. Kim, X. H. Hu, B. Sinha, and C. G. Kim, J. Magnetics **17**, 302 (2012).
[12] B. Sinha, S. Anandakumar, S. Oh, and C. Kim, Sens. Actuators A **182**, 34 (2012).
[13] R. Venu, B. Lim, X. H. Hu, I. Jeong, T. S. Ramulu, and C. G. Kim, Microfludics and Nanofludics **14**, 277 (2013).